Optimizing Stabilizer Parities for Improved Logical Qubit Memories

Dripto M. Debroy, Laird Egan, Crystal Noel, Andrew Risinger, Daiwei Zhu, Debopriyo Biswas, Marko Cetina, Chris Monroe, and Kenneth R. Brown

Optimizing Stabilizer Parities for Improved Logical Qubit Memories

Dripto M. Debroy,[1, *] Laird Egan,[2] Crystal Noel,[1, 2, 3] Andrew Risinger,[2] Daiwei Zhu,[2]
Debopriyo Biswas,[2] Marko Cetina,[1, 2] Chris Monroe,[1, 2, 3, 4] and Kenneth R. Brown[1, 3, †]

[1]*Department of Physics, Duke University, Durham, NC 27708, USA*
[2]*Joint Quantum Institute, Center for Quantum Information and Computer Science,
and Departments of Physics and Electrical and Computer Engineering,
University of Maryland, College Park, MD 20742, USA*[‡]
[3]*Department of Electrical and Computer Engineering, Duke University, Durham, NC 27708, USA*
[4]*IonQ, College Park, MD 20740, USA*

We study variants of Shor's code that are adept at handling single-axis correlated idling errors, which are commonly observed in many quantum systems. By using the repetition code structure of the Shor's code basis states, we calculate the logical channel applied to the encoded information when subjected to coherent and correlated single qubit idling errors, followed by stabilizer measurement. Changing the signs of the stabilizer generators allows us to change how the coherent errors interfere, leading to a quantum error correcting code which performs as well as a classical repetition code of equivalent distance against these errors. We demonstrate a factor of 3.78 ± 1.20 improvement of the logical $T2^*$ in a distance-3 logical qubit implemented on a trapped-ion quantum computer. Even-distance versions of our Shor code variants are decoherence-free subspaces and fully robust to identical and independent coherent idling noise.

In quantum error correction, coherent errors are unwanted unitary operations applied to the physical qubits. Unlike stochastic errors, which scale linearly, coherent errors build up quadratically [1, 2, 15]. Coherent errors of various types can be mitigated through composite pulse sequences [3–5], random compiling [6, 7], and circuit compilation [8, 9].

We consider errors resulting from spatially or temporally correlated phase noise. Such noise can arise from magnetic field fluctuations or instabilities in timing systems, which are a concern in most architectures, including trapped ions, superconductors, neutral atoms, and nitrogen-vacancy diamonds [10]. For optically addressed qubits, this type of noise can also appear due to beam path length fluctuations or finite laser linewidth [11]. Although error correction suppresses these errors [12, 13], they can increase logical qubit error relative to stochastic errors.

Previous work on temporally correlated idling error, also called coherent idling error, has focused on finding thresholds below which the coherence of the resulting logical channel is reduced [14, 15]. In Ref. [15], the authors present an exact solution for the logical channel experienced by a repetition code under coherent idling error. We use this model to solve for the exact logical channels for a set of variants of Shor's 9-qubit code [16]. Standard stabilizer codes stabilize even parity states. By changing the parity that a stabilizer preserves, we can directly control how the coherent errors interfere. In this way, we can create codes where significant fractions of the coherent errors cancel out, similar to non-stabilizer code

constructions [17]. Even-distanced versions of our coherent error resilient code are members of the code family described in Ref. [18], and fully cancel homogenous coherent idling error. The codespaces of these Shor-codes exist inside of a decoherence-free subspace [19–23].

Our calculations follow the example presented in Ref. [15]. Consider an error model where all qubits are rotated along the Z axis by an angle θ, represented by the channel $\mathcal{N}_\theta(\rho)$ on an n qubit density matrix ρ:

$$
\begin{aligned}
\mathcal{N}_\theta(\rho) &= Z(\theta)^{\otimes n} \rho (Z(\theta)^\dagger)^{\otimes n}, \\
Z(\theta) &= e^{-i\theta Z/2},
\end{aligned}
\tag{1}
$$

Now assume that the qubits are being used to encode one classical bit of information in a rotated n-bit repetition code:

$$
\begin{aligned}
|+\rangle_L &= |+\rangle^{\otimes n} = 2^{n/2}(|0\rangle + |1\rangle)^{\otimes n}, \\
|-\rangle_L &= |-\rangle^{\otimes n} = 2^{n/2}(|0\rangle - |1\rangle)^{\otimes n}.
\end{aligned}
\tag{2}
$$

Once the error in Eq. 1 has been applied, a round of stabilizer measurements are taken, where the stabilizer generators of the repetition code are:

$$
S_{rep} = \langle X_0 X_1, X_1 X_2, \ldots X_{n-2} X_{n-1} \rangle.
$$

Every syndrome corresponds to two Z-type errors, related by $E_1 = E_2 Z_L$, where $Z_L = Z^{\otimes n}$ and $\{E_1, E_2\}$ are Z-type errors. The correction applied is chosen to be the lower-weight error, which is optimal if $\sin^2(\theta/2) < 1/2$. If we define $\alpha_s(\beta_s)$ as the prefactor to the corrected(uncorrected) Pauli error corresponding to a syndrome s in an expansion of Eq. 1, the logical channel after correction is [15]:

$$
\begin{aligned}
\mathcal{N}_L(\rho) &= \sum_s (\alpha_s I_L + \beta_s Z_L)\rho(\alpha_s^* I_L + \beta_s^* Z_L), \\
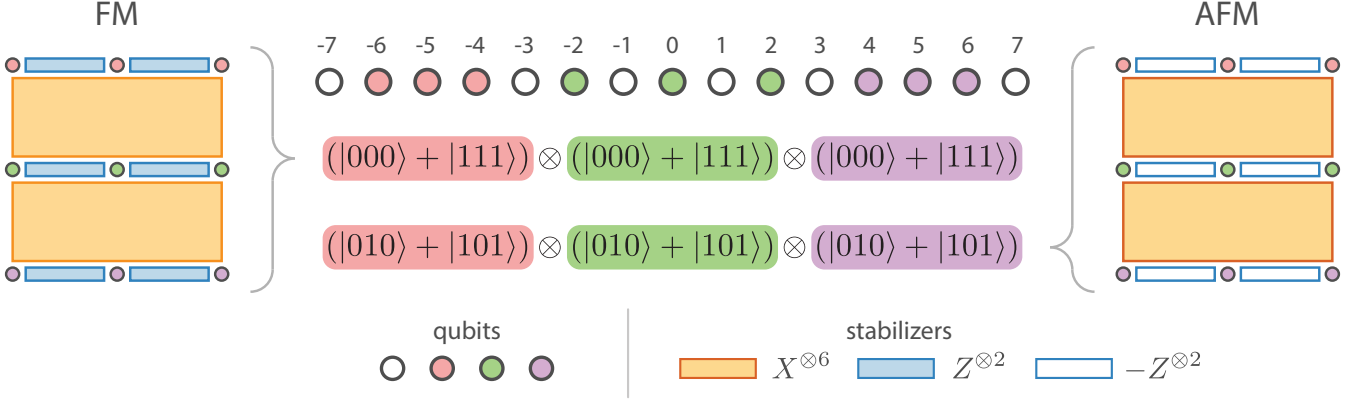&= \sum_s P_s \bar{Z}(\theta_s)\rho\bar{Z}(\theta_s)^\dagger.
\end{aligned}
\tag{3}
$$

FIG. 1: Diagrams for the ferromagnetic (left) and anti-ferromagnetic (right) [[9,1,3]] Shor's codes, as well as an ion chain with labeled ion indices. The qubit state representing $|0\rangle_L$ is shown for each variant, with each GHZ state color coded to match the ions in the chain as well as their location in the code diagrams. The qubits in each GHZ state are ordered from left to right.

$$Z_L(\theta) \equiv e^{-i\theta Z_L/2},$$
$$P_s \equiv |\alpha_s|^2 + |\beta_s|^2, \qquad (4)$$
$$\theta_s \equiv 2\arctan\left(\frac{i\beta_s}{\alpha_s}\right).$$

As an example in a 3-bit repetition code, the syndrome outcome of 01 could be caused by an error IIZ or an error ZZI. The weight-1 error IIZ is corrected, leading to

$$\alpha_{01} = \cos(\theta/2)^2(-i\sin(\theta/2)),$$
$$\beta_{01} = \cos(\theta/2)(-i\sin(\theta/2))^2. \qquad (5)$$

These amplitudes imply a rotation angle of

$$\theta_{01} = 2\arctan\left(\frac{\sin(\theta/2)}{\cos(\theta/2)}\right) = \theta, \qquad (6)$$

meaning that the logical rotation angle for this syndrome is the physical rotation angle.

This is not always true, and as shown in Eq. 3, the logical Z rotation is conditional on the syndrome outcome measured. In the case of an n-bit repetition code, the values of α_s and β_s only depend on n and the weights of the corresponding errors, and are completely independent of the error arrangement. Consequently, one can define the quantities:

$$P_{n,w}(\theta) = \binom{n}{w}((\cos(\theta/2)^{(n-w)}\sin(\theta/2)^w)^2$$
$$+ (\cos(\theta/2)^w \sin(\theta/2)^{(n-w)})^2), \qquad (7)$$

$$\theta_{n,w} = (-1)^{(n-2w-1)/2}2\arctan(\tan^{n-2w}(\theta/2)),$$

where n is the distance, and w is the weight of the correctable (lower weight) error. The logical channel in Eq. 3

can then be rewritten as:

$$\mathcal{N}_L(\theta) = \sum_{w=0}^{(n-1)/2} P_{n,w}(\theta)Z_L(\theta_{n,w})\rho Z_L(\theta_{n,w})^\dagger. \qquad (8)$$

This compact description of the logical channel relies on the simple construction of the repetition code. For most quantum error correcting codes, syndromes do not translate as directly into easily understood errors. We study the case of Shor's codes, which follow this structure. The 9-qubit code presented in Ref. [16] can be written as three 3-bit repetition codes with Z-type stabilizers, concatenated into a repetition code with X-type stabilizers. The resulting code, with 6 weight-2 Z-type stabilizers and 2 weight-6 X-type stabilizers, has logical states which are products of Greenberger-Horne-Zeilinger (GHZ) states:

$$|0\rangle_L \equiv \frac{1}{2\sqrt{2}}(|000\rangle + |111\rangle)^{\otimes 3},$$
$$|1\rangle_L \equiv \frac{1}{2\sqrt{2}}(|000\rangle - |111\rangle)^{\otimes 3}. \qquad (9)$$

We consider this code, as well as a variant with Z-type stabilizer generators of opposite parity. In Appendix A, we discuss the pair of codes created by taking these two codes and swapping the stabilizer bases.

On the left of Fig. 1 is the standard 9-qubit Shor's code. The logical state preparation and measurement of this code has been demonstrated with trapped ions [24, 25] and photons [26]. The phase errors on a given GHZ state combine constructively, as can be seen for the states shown in Eq. 9. This is a consequence of the ZZ stabilizers along each row, which lead to $Z(\theta)$ errors being indistinguishable for qubits on the same row. We can imagine pushing all the errors to the leftmost column of qubits, which will each experience a rotation of angle

$n\theta$. The outer repetition code will have the same logical channel as Eq. 8, with $\theta \rightarrow n\theta$:

$$\mathcal{N}_L(\theta) = \sum_{w=0}^{(n-1)/2} P_{n,w}(n\theta) Z_L(n\theta_{n,w}) \rho Z_L(n\theta_{n,w})^\dagger. \quad (10)$$

This represents a worst-case situation where the logical qubit experiences an error that increases quadratically with distance n.

We now consider the code on the right of Fig. 1, which we will refer to as the anti-ferromagnetic case since the GHZ states composing its logical states resembles the ground states of an anti-ferromagnetic Ising spin chain. This code has the same stabilizer structure as that on the left of Fig. 1, but with the ZZ stabilizers negated. This does not impact on the code's ability to correct stochastic errors, but causes the interference of the coherent idling errors to go from constructive to destructive. In the even-distance case, all the errors cancel out. These codes are immune to errors described by Eq. 1, and are an example of the codes described in Ref. [18]. For the odd-distanced cases, a single error does not cancel on each row. The resulting effective error channel seen by the outer repetition code is identical to that seen in the classical repetition code case, so the logical error channel is identical to that seen in Eq. 8. This represents a significant improvement in the logical error channel, as the repetition code has the maximum possible threshold of $p_{th} = 1/2$ [?].

Our discussion above assumes temporal and spatial correlation, but these modified codes also improve protection for errors that are only spatially correlated. This follows from previous work on correlated dephasing noise in the context of weak decoherenece free subspaces [27]. Here we do not seek perfect cancellation of correlated errors, but a linear reduction in the error rate.

We confirm these results on a trapped ion quantum computer that has previously demonstrated fault-tolerant error-correction protocols [24]. A chain of 15 ions is trapped above a microfabricated chip trap [28], with optical individual site addressing controlled by a multi-channel acousto-optic modulator. Measurement, single-qubit gate, and two-qubit gate fidelities are $> 99.5\%$, 99.98%, and 98.5% respectively [24]. The qubit in this system is defined on the electronic ground state hyperfine "clock" states of $^{171}\text{Yb}^+$ ions with angular momentum F and projection m_f: $|0\rangle \equiv |F = 0; m_F = 0\rangle$, $|1\rangle \equiv |F_1; m_F = 0\rangle$. The qubit frequency is $\omega_0 = 2\pi \times (12, 642, 812, 118.5 \text{ Hz} + \delta_2)$, where $\delta_2 = (310.8)B^2$ Hz is the second-order Zeeman shift for a magnetic field B in Gauss [29].

In our system, residual second-order sensitivity to magnetic fluctuations and/or local oscillator noise limits the T_2 decoherence time to ≈ 2.75 s, whereas the qubit itself is capable of $T_2 > 1$ hour [30]. The relevant quantity for this paper is the un-echoed $T_2^* = 0.6$ s decoherence time using optical control of the qubits, likely dominated by mechanical vibrations that shift the phase of the optical standing wave relative to the ion. In contrast to phase noise, there is also a well-characterized static linear magnetic field gradient across the length of ion chain that results in a qubit frequency shift of ± 4 Hz shift relative to the center ion. In Ref. [24] the chip was rotated so that the magnetic field was constant throughout the chip, as opposed to the linearly varying magnetic field in this geometry. If this shift is not accounted for in software then it will create relative phase shifts between the ions that also appear as a coherent idling error.

We first study the individual ferromagnetic and anti-ferromagnetic GHZ states which compose the logical states. These states are:

$$|FM_n\rangle = \frac{1}{\sqrt{2}} \left(|000\ldots\rangle + |111\ldots\rangle \right),$$
$$|AFM_n\rangle = \frac{1}{\sqrt{2}} \left(|010\ldots\rangle + |101\ldots\rangle \right), \quad (11)$$

A code with $n \times n$ qubits has a logical state which is a tensor product of n of these states. The logical states and ion-to-qubit mappings for the [[9,1,3]] ferromagnetic and anti-ferromagnetic Shor's codes are shown in Fig. 1.

After these states are prepared, we perform a Ramsey experiment with variable wait time to measure the coherence of the state as a function of time, as in Ref. [24]. The result of this experiment for different GHZ sizes is shown in Fig. 2, where the contrast corresponds to $\langle X^{\otimes n}\rangle$. For the ferromagnetic states in Fig. 2a, we observe an initial fast decay of the contrast on a timescale that corresponds to the correlation time of phase noise in our system, followed by a longer slow decay. The anti-ferromagnetic states in Fig. 2b, exhibit only a slow decay, indicating that these states are more resistant to the correlated phase errors present in the system. Using these states allows the code to inherit their robustness. While the 4-qubit AFM GHZ state is predicted to be completely insensitive to our dominant idling error, we do observe a small decay over 10 ms, indicating small contributions from a other error sources. The additional entangling gates penalize the larger GHZ states, and as shown the increased robustness to coherent idling error is not quite enough to outweigh this cost for the 4-qubit AFM state.

We now directly compare the performance of [[9,1,3]] FM and AFM Shor's codes in Fig. 3, using a logical qubit Ramsey experiment identical to the one performed in Ref. [24]. In this experiment, three separate 3-qubit GHZ states are constructed, as shown in Fig. 1. Using the structure of the codestates, we apply one round of error correction based off the measurement outcomes of the data qubits [24], leading to the three curves in Fig. 3. Raw curves are constructed by the total parity of the 9 data qubits after a measurement in the X basis, error corrected curves reconstruct the stabilizer outcomes from these measurements and apply one correction, while error detected curves reconstruct these stabilizer outcomes and then discard any run in which the stabilizers are violated. In this manner, error correction corresponds to "post-processing" of the data, whereas error detection
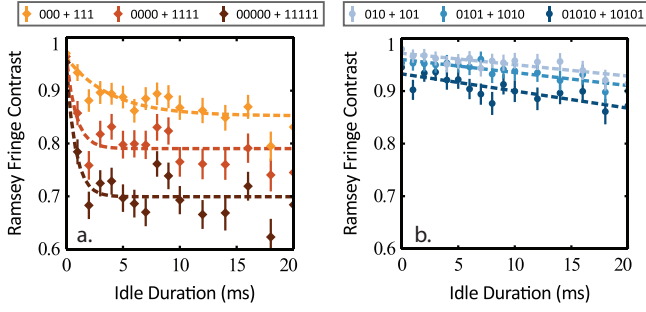
FIG. 2: Fringe contrast after a Ramsey experiment on the (a) ferromagnetic and (b) anti-ferromagnetic GHZ states for different distances. The dashed lines are present to serve as guides to the eye.
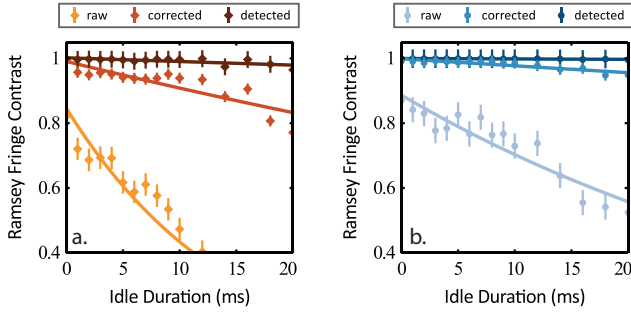

FIG. 3: Experimental dephasing performance of (a) ferromagnetic and (b) anti-ferromagnetic [[9, 1, 3]] Shor's code logical states. The Ramsey fringe amplitude gives the coherence of the states. The data is fit to $A \exp(-\Gamma t)$, where Γ is $1/\tau$, the lifetime of the state. Fitting parameters are presented in Appendix B.

FIG. 4: Individual GHZ state Ramsey fringes after a 20 ms wait time for the (a) ferromagnetic and (b) anti-ferromagnetic [[9,1,3]] Shor's code $|0\rangle_L$ logical states. Colors are selected to match the GHZ state coloring from Fig. 1. The data is fit to $A \cos(3\phi + \phi_0)$. Fitting parameters are presented in Appendix B.

corresponds to "post-selection" of the data. A single error on the data qubits flips the outcome of the raw data, two errors are required to flip the outcome of the corrected data, and three errors are needed to flip the outcome of the detected data. The ferromagnetic code performs worse than the anti-ferromagnetic code in all three cases. We can calculate logical $T2^*$ times of 115(10) ms in the ferromagnetic case and 450(150) ms in the antiferromagnetic case.

The logical states presented in Eq. 9 are composed of three separate GHZ states, allowing us to study their performance separately in Fig. 4. The reduction in contrast for the central AFM GHZ state is due to lower gate fidelities in its preparation circuit, not coherent error. By considering the spatial arrangement of the GHZ states, as shown in Fig. 1, we can study the impact of the static magnetic field gradient on the code. Any state which balances the number of excitations in each GHZ state is resilient to dynamic noise of the form described in Eq. 1 and shown in Fig. 2. Our particular mapping, however, is also robust to magnetic fields which slowly vary in space because our states have errors cancel with their nearest neighbors. In Fig. 4, we see that the mag-
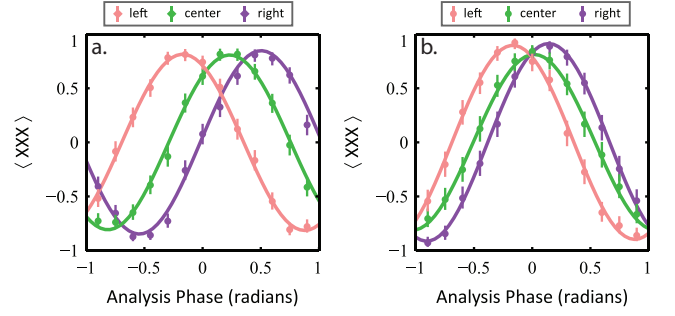
netic field appears to vary linearly across the axis of the trap, leading to GHZ states experiencing different phase shifts depending on their position in the chain. While this error does not decrease the coherence of individual GHZ states, the performance of the code depends on the three GHZ states remaining in phase with each other. The physical states shown in Fig. 4a, which correspond to the FM code in Fig. 1, experience higher relative phase shifts than their AFM counterparts in Fig. 4b. If we assume that the magnetic field is linearly increasing along the chain, we can define the angle of a qubit at integer position x as

$$\theta_x = \theta_0 + x\delta, \tag{12}$$

where δ is the difference in phase between a qubit in position x and the one in $x + 1$, and θ_0 is the phase accumulated by the central ion. Under these conditions, the phase accumulated for the FM GHZ states in Fig. 1 would be:

$$\begin{aligned} \theta_{\text{left}} &= \theta_{-6} + \theta_{-5} + \theta_{-4} = 3\theta_0 - 15\delta, \\ \theta_{\text{center}} &= \theta_{-2} + \theta_0 + \theta_2 = 3\theta_0, \\ \theta_{\text{right}} &= \theta_4 + \theta_5 + \theta_6 = 3\theta_0 + 15\delta. \end{aligned} \tag{13}$$

In comparison, the phase accumulated for the AFM GHZ states would be:

$$\begin{aligned} \theta_{\text{left}} &= \theta_{-6} - \theta_{-5} + \theta_{-4} = \theta_0 - 5\delta, \\ \theta_{\text{center}} &= \theta_{-2} - \theta_0 + \theta_2 = \theta_0, \\ \theta_{\text{right}} &= \theta_4 - \theta_5 + \theta_6 = \theta_0 + 5\delta, \end{aligned} \tag{14}$$

corresponding to a threefold reduction in accumulated phase for the individual GHZ states. These accumulated phases take the place of θ in Eq. 3 when error correction is applied using a distance-3 code. A threefold reduction in accumulated phase would correspond to an approximately 81-fold reduction in logical error rate, assuming no other error sources existed in the system.

In Appendix C we discuss a variation on this experiment which allowed us to experimentally confirm our understanding of the magnetic fields present in our system. Of course, if the magnetic fields are static and well known, a preferable option would be to adjust the qubit frequencies in classical control. However this option is not possible for unknown drifts which may occur during a computation. Additionally, in trapped-ion architectures that involve extensive shuttling operations [**?**], qubits will acquire a path dependant phase that needs to be calibrated and pre-calculated. Codes robust to this error may reduce calibration overheads and circuit compilation complexity.

Our primary conclusion is that changing stabilizer parity allow us to control the interference between correlated idling errors. We present a family of codes, which we refer to as anti-ferromagnetic Shor's codes, which inherit the one sided threshold of standard Shor's codes while also possessing a threshold against correlated idling noise in the other basis. The even-distanced versions of our code family are an example of the codes described in Ref. [18]. The particular choice of qubit mapping we use also idling errors which are slowly varying in space. Such idling-resistant codes could be used in a concatenated scheme much like the one discussed in Ref. [17]. We present experimental data from a trapped-ion quantum computer which demonstrates our codes showing marked improvements in performance relative to the standard Shor's code. We can also change parities preserved by higher weight stabilizers, as considered in Appendix A, leading to less drastic cancellations. These modifications still leave error correcting performance against uncorrelated stochastic errors unchanged, while improving the resilience to correlated idling error, and could be implemented for any CSS code.

I. ACKNOWLEDGEMENTS

[1] R. Kueng, D. M. Long, A. C. Doherty, and S. T. Flammia, Physical Review Letters **117**, 170502 (2016).

[2] D. Greenbaum and Z. Dutton, Quantum Science and Technology **3**, 015007 (2017).

[3] L. Viola, E. Knill, and S. Lloyd, Physical Review Letters **82**, 2417 (1999).

[4] J. A. Jones, Physical Review A **67**, 012317 (2003).

[5] K. R. Brown, A. W. Harrow, and I. L. Chuang, Physical Review A **70**, 052318 (2004).

[6] J. J. Wallman and J. Emerson, Physical Review A **94**, 052325 (2016).

[7] E. Campbell, Physical Review Letters **123**, 070503 (2019).

[8] D. M. Debroy, M. Li, M. Newman, and K. R. Brown, Phys. Rev. Lett. **121**, 250502 (2018).

[9] Z. Cai, X. Xu, and S. C. Benjamin, npj Quantum Information **6**, 1 (2020).

[10] H. Ball, W. D. Oliver, and M. J. Biercuk, npj Quantum Information **2**, 1 (2016).

[11] A. Bermudez, X. Xu, M. Gutiérrez, S. C. Benjamin, and M. Müller, Phys. Rev. A **100**, 062307 (2019), URL https://link.aps.org/doi/10.1103/PhysRevA.100.062307.

[12] S. Beale, J. Wallman, M. Gutiérrez, K. R. Brown, and R. Laflamme, Physical Review Letter **121**, 190501 (2018).

[13] E. Huang, A. C. Doherty, and S. Flammia, Physical Review A **99**, 022313 (2019).

[14] S. Bravyi, M. Englbrecht, R. Koenig, and N. Peard, npj Quantum Inf. **4** (2018).

[15] J. K. Iverson and J. Preskill, New Journal of Physics **22**, 073066 (2020).

[16] P. W. Shor, Phys. Rev. A **52**, R2493 (1995).

[17] Y. Ouyang, arXiv preprint arXiv:2010.00538 (2020).

[18] J. Hu, Q. Liang, N. Rengaswamy, and R. Calderbank, arXiv preprint arXiv:2011.00197 (2020).

[19] D. A. Lidar, I. L. Chuang, and K. B. Whaley, Physical Review Letters **81**, 2594 (1998).

[20] E. Knill, R. Laflamme, and L. Viola, Phys. Rev. Lett. **84**, 2525 (2000), URL https://link.aps.org/doi/10.1103/PhysRevLett.84.2525.

[21] D. Kielpinski, V. Meyer, M. Rowe, C. A. Sackett, W. M. Itano, C. Monroe, and D. J. Wineland, Science **291**, 1013 (2001).

[22] Z. Deng, M. Feng, and K. Gao, Physical Review A **75**, 024302 (2007).

[23] R. W. Andrews, C. Jones, M. D. Reed, A. M. Jones, S. D. Ha, M. P. Jura, J. Kerckhoff, M. Levendorf, S. Meenehan, S. T. Merkel, et al., Nature nanotechnology **14**, 747 (2019).

[24] L. Egan, D. M. Debroy, C. Noel, A. Risinger, D. Zhu, D. Biswas, M. Newman, M. Li, K. R. Brown, M. Cetina, et al., arXiv preprint arXiv:2009.11482 (2020).

[25] N. H. Nguyen, M. Li, A. M. Green, C. H. Alderete, Y. Zhu, D. Zhu, K. R. Brown, and N. M. Linke, arXiv preprint p. arXiv:2104.01205 (2021).

[26] Y.-H. Luo, M.-C. Chen, M. Erhard, H.-S. Zhong, D. Wu, H.-Y. Tang, Q. Zhao, X.-L. Wang, K. Fujii, L. Li, et al., arXiv preprint (2020), 2009.06242.

[27] J. Kempe, D. Bacon, D. A. Lidar, and K. B. Whaley, Physical Review A **63** (2001), ISSN 1094-1622, URL

http://dx.doi.org/10.1103/PhysRevA.63.042307.

[28] P. L. W. Maunz, Sandia National Laboratories Report No. SAND2016-0796R (2016), URL http://prod.sandia.gov/techlib/access-control.cgi/2016/160796r.pdf.

[29] P. T. Fisk, M. J. Sellars, M. A. Lawn, and G. Coles, IEEE transactions on ultrasonics, ferroelectrics, and frequency control **44**, 344 (1997).

[30] P. Wang, C.-Y. Luan, M. Qiao, M. Um, J. Zhang, Y. Wang, X. Yuan, M. Gu, J. Zhang, and K. Kim, Nature Communications **12**, 233 (2021).

[31] J. M. Pino, J. M. Dreiling, C. Figgatt, J. P. Gaebler, S. A. Moses, C. Baldwin, M. Foss-Feig, D. Hayes, K. Mayer, C. Ryan-Anderson, et al., arXiv preprint arXiv:2003.01293 (2020).